Front. Phys. 13(3), 138105 (2018)
https://doi.org/10.1007/s11467-018-0752-8

REVIEW ARTICLE

Recent progress on borophene: Growth and structures

Longjuan Kong[1,2], **Kehui Wu**[1,2,3], **Lan Chen**[1,2,†]

[1] *Institute of Physics, Chinese Academy of Sciences, Beijing 100190, China*
[2] *School of Physics, University of Chinese Academy of Sciences, Beijing 100049, China*
[3] *Collaborative Innovation Center of Quantum Matter, Beijing 100871, China*
Corresponding author. E-mail: [†] *lchen@iphy.ac.cn*
Received January 20, 2018; accepted February 8, 2018

Boron is the neighbor of carbon on the periodic table and exhibits unusual physical characteristics derived from electron-deficient, highly delocalized covalent bonds. As the nearest neighbor of carbon, boron is in many ways similar to carbon, such as having a short covalent radius and the flexibility to adopt sp^2 hybridization. Hence, boron could be capable of forming monolayer structural analogues of graphene. Although many theoretical papers have reported finding two-dimensional allotropes of boron, there had been no experimental evidence for such atom-thin boron nanostructures until 2016. Recently, the successful synthesis of single-layer boron (referred to as borophene) on the Ag(111) substrate opens the era of boron nanostructures. In this brief review, we will discuss the progress that has been made on borophene in terms of synthetic techniques, characterizations and the atomic models. However, borophene is just in infancy; more efforts are expected to be made in future on the controlled synthesis of quality samples and tailoring its physical properties.

Keywords borophene, molecular beam epitaxy, scanning tunneling microscopy, atomic model, density functional theory

PACS numbers 68.55.-a, 61.46.-w, 81.05.Zx, 68.37.Ef, 81.15.Hi

Contents

1 Introduction 1
2 Synthesis and characterization 4
2.1 Two-dimensional boron monolayer 4
2.2 Borophene nanoribbons 6
3 Atomic structures of synthesized 2D boron 7
4 Summary 9
Acknowledgements 9
References and notes 9

1 Introduction

Graphene, the first planar sheet of which was produced by Novoselov and Geim in 2004 [1], has inspired the development of a so-called flatland of two-dimensional (2D) materials with complementary properties and functionalities enabling rapid advances in science and engineering, and an accelerated global development in nanotechnology applications that can address societal challenges in energy, electronics, sensors and health [2–5]. As the chemical properties of elements are determined by their valence electrons, silicon, germanium, and tin all belonging to same group IV in the periodic table may show similarity to carbon in forming graphene-like monolayer sheets [6]. Indeed, the Si-based silicene [7–10], Ge-based germanene [11–13], and Sn-based stanene [14–17] have been to be stable and realized by molecular beam epitaxy (MBE) growth in ultrahigh vacuum. Although the graphene-like 2D materials based on Si, Ge, or Sn follow the hexagonal honeycomb structure analogous to graphene, their most stable form is a buckled honeycomb lattice due to their larger interatomic distances [6, 18, 19]. The buckled structure resulting from larger interatomic distances and the strong spin-orbit coupling (SOC) pave a pathway for accessing the new quantum state of matter known as a 2D topological insulator [20]. However, these 2D materials are susceptible to oxidation when exposed to the air and are limited in building nanoscale devices.

Hence, the pursuit of alternative versatile 2D graphene-like materials for the development of material science and the future of nano-electronics is ongoing.

*Special Topic: Inorganic Two-Dimensional Nanomaterials (Eds. Changzheng Wu & Xiaojun Wu).

The element boron, positioned just to the left of carbon in the periodic table, has a striking similarity to carbon, from planar clusters [21–25] and cage-like fullerences [26–30] to one dimensional (1D) nanotubes [31–33], which motivates an exploration of monoatomic-layer 2D boron (named as borophene). As the fifth element in the periodic table, boron has three valence electrons with the ground-state configuration of $2s^2 2p^1$, whereas it has four available valence orbitals achieved by promoting an electron from the $2s$ to the $2p$ orbital. It is at once clear that there are more usable atomic orbitals than number of electrons. This prevents the fulfilment of the octet rule, resulting in the electron-deficient state of the boron atom. This means there are not enough electrons in the boron atom to fill all electron orbitals in a chemical bond based on the classic two-centered two-electron (2c-2e) bonds used in carbon systems. Therefore, the coexistence of localized 2c-2e and delocalized multicenter two-electron (nc-2e) bonds is required to resolve the electron deficiency and stabilize the boron crystals (Fig. 1). This unique nature enables boron to form complex polymorphic bulk structures and nanoscopic clusters as well as a large number of compounds with different elements [22, 34, 35]. The multicenter bonds and electron-deficient features of boron make the synthesis of 2D boron challenging. This can be understood imagining that the multicenter bonds of boron are energetically competitive and will cause boron atoms to assemble into various polymorphs. Therefore, a 2D boron sheet may generally be a fluxional system [36].

Thus, extensive theoretical efforts have been devoted to exploring the 2D boron sheet. As early as 1997, Boustani predicted that the quasi-planar 2D boron sheet could be constructed from a basic unit of puckered B_7 cluster [Fig. 2(a)], using the systematic ab initio density functional method [37, 38]. This study caused increased interest in finding out the free-standing monolayer structure of boron. A prediction of the stable buckled triangular network of B atoms has been confirmed by Cabria *et al.* using first-principle calculations (Fig. 2(b)) [39–

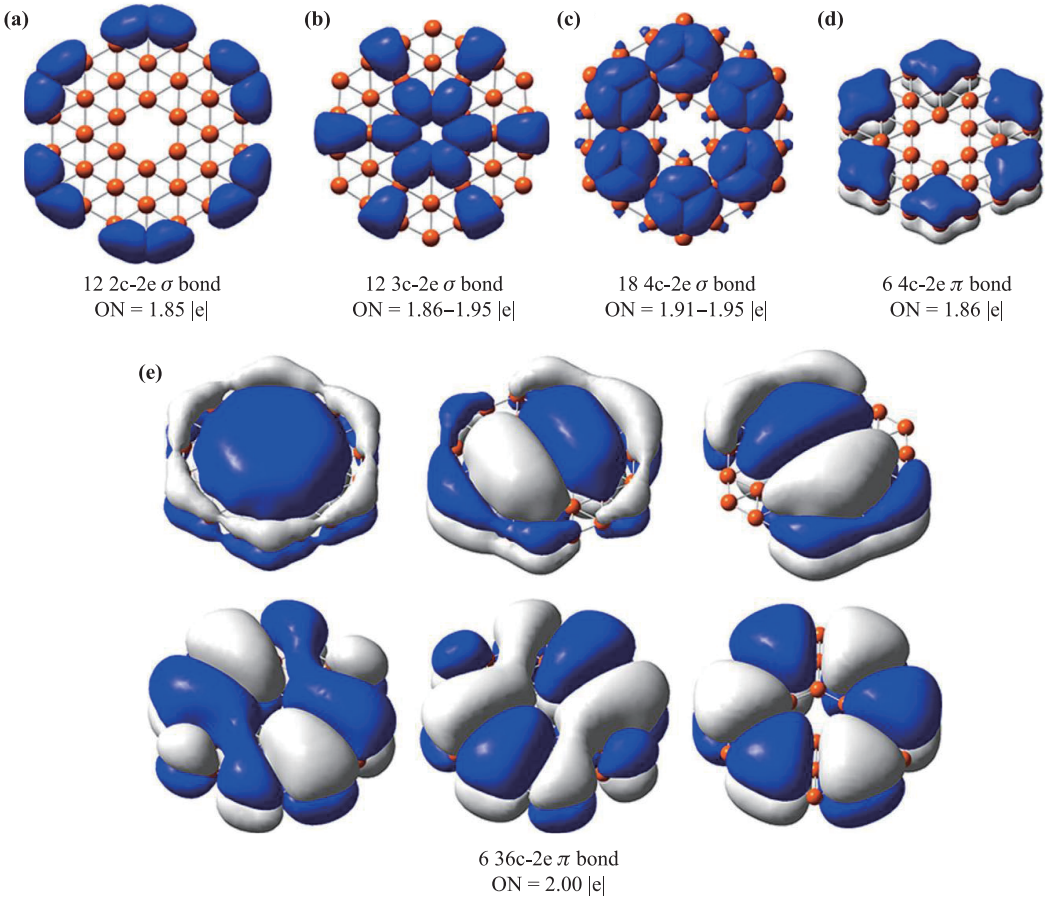

Fig. 1 Chemical bonding analysis for the hexagonal C_{6v} structure of B_{36}. **(a)** Localized σ bonding of peripheral B-B bonds. **(b–e)** Delocalized multicenter two-electron (nc-2e). The analysis was performed using the adaptive natural density partitioning (AdNDP) method, which localizes the computed density matrix into n-centre two-electron (nc-2e) bonds, with n ranging from one to the total number of atoms in the molecule. ON stands for occupation number and is equal to 2.00 |e| (meaning a density of exactly two electrons) in the ideal case. Reproduced from Ref. [24].

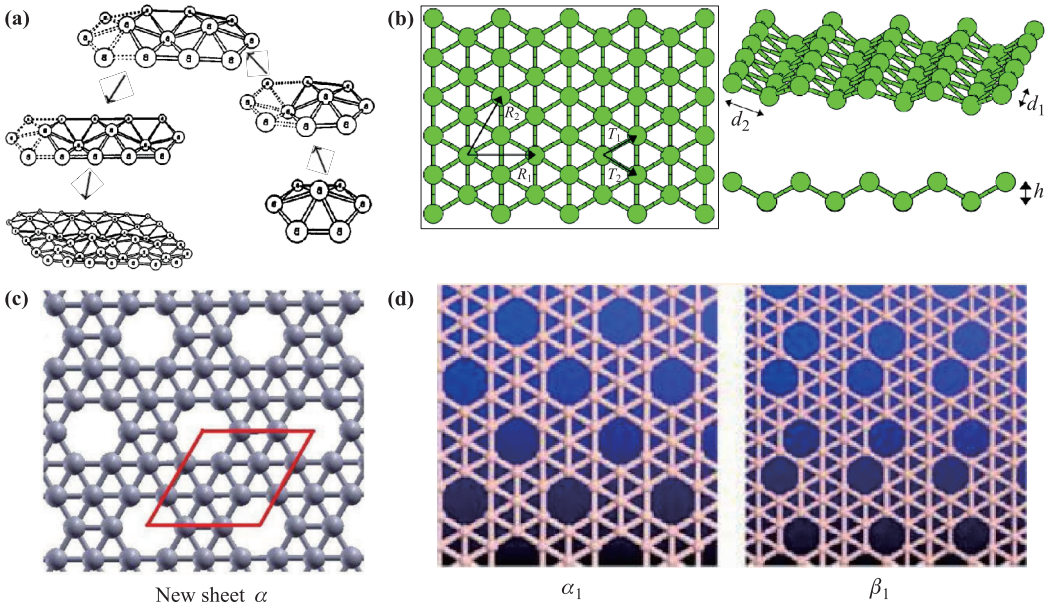

Fig. 2 Illustration of structures of the monolayer boron sheet. **(a)** The schematic diagram of the growth from B7 cluster to quasiplanar 2D boron sheet. **(b)** Optimized buckled triangular boron sheet from different perspectives. **(c)** Optimized α boron sheet. **(d)** Low-energy structures of α_1- and β_1-sheets. The panels **(a)**, **(b)**, **(c)**, and **(d)** were reproduced from Refs. [37, 41, 43, 45], respectively.

41]. However, the mixed hexagonal-triangular 2D boron sheet [the α-sheet illustrated in Fig. 2(c)] proposed by Tang and Ismail-Beigi was thought to be the more stable than one composed only of buckled triangular motifs [42–44]. In 2012, through an extensive structural search using the first-principle particle-swarm optimization global algorithm, Zeng's group [45] found that two flat monolayers — α_1- and β_1-sheets, shown in Fig. 2(d) — are the most stable 2D boron structures among the state-of-the-art 2D structures including the α-sheet and the sub-sheets reported by Yakobson's group [46]. All these flat 2D boron sheets have periodic hexagonal holes incorporated in the triangular lattice, which can be explained by a chemical bonding diagram where hexagonal holes are prone to accepting electrons as scavengers of extra electrons from the flat triangular regions. Thus, the stability of the flat monolayer boron structure depends strongly on the hexagonal hole density η [43]. To date, experimental evidence of flat nanostructured boron is rare. On the other side, the planar B_{36} cluster with a central hexagonal hole has been determined experimentally, providing the first experimental support for the viability of atom-thin boron sheets [24].

In these theoretical works, many freestanding 2D boron structures were proved to adopt a quasi-planar configuration, but the 2D boron structure may be created experimentally via the deposition growth process on a suitable substrate. Thus, a more extensive investigation of substrate selection and the corresponding effects on the boron structures is required. In 2013, Yakobson and collaborators explored the possibility of synthesizing a 2D boron sheet on metaland metal-boride substrates by first-principle calculations. It suggested that the deposition of boron on Ag(111) or Au(111) surfaces can result in 2D boron [47]. In the same year, the superiority of the Cu(111) substrate for the growth of borophene was theoretically predicted by Zhao *et al.* in terms of the low diffusion barrier of a single boron atom on a Cu(111) surface and the monotonic decrease of formation energy during the growth process [48]. Additionally, Gao *et al.* have considered the computationally possible synthesis of three types of single-layer boron sheets on different metal surfaces. It suggested that a hexagonal boron sheet similar to graphene in geometry can be formed on an Al(111) surface due to the electron transfer from the metal substrate to the boron sheet [49].

Studies on borophene relied primarily on theoretical predictions until recent investigations experimentally demonstrated borophene synthesis on Ag(111) substrates. The first experimental attempt to synthesize borophene on Ag(111) substrates by molecular beam epitaxy (MBE) in ultrahigh vacuum was performed by Chen and Wu *et al.* [50]. Another parallel work was reported by Mannix *et al.*, showing very similar results [51]. The successful synthesis of borophene brings a new member to the wonderful 2D materials family and paves the way to exploring boron-based microelectronic devices. However, the research of borophene is just in its infancy,

and a lot of properties remain to be explored before borophene can be established as a valuable alternative for the next generation of electronic applications.

Following the experimental realization of borophene, this brief review will introduce the current progress in the exploration of 2D boron. Here, we will focus on experimental results and analysis combined with some theoretical calculations. We will provide a brief overview on the development of borophene, in the hope that more researchers will research this new and interesting 2D atomic crystal. The rest of this article is organized as follows: the experimental synthesis and relevant characterization of boron sheets on Ag(111) surfaces is introduced in Section 2. In Section 3, the detailed description of their atomic structures is presented. Section 4 provides a brief summary.

2 Synthesis and characterization

2.1 Two-dimensional boron monolayer

Unlike the naturally layered structures of bulk graphite and black phosphorus, boron does not have a natural 3D allotrope with a layered structure. Thus, micromechanical exfoliation is not suitable to the production of borophene. On the contrary, molecular beam epitaxy (MBE) is a powerful technique for producing high-quality and large-area atomically flat sheets on substrates. Consequently, borophene was experimentally realized by directly evaporating boron atoms onto a clean single-crystal Ag(111) surface with suitable substrate temperature. Feng *et al.* showed that 2D boron sheets with two distinct structures defined as S1 phase and S2 phase can be formed epitaxially on Ag(111) surfaces, which was confirmed by scanning tunneling microscopy (STM) (Fig. 3) [50].

When the substrate temperature is lower than 570 K during growth, only clusters and disordered boron are obtained on the surface. Once the temperature reaches about 570 K, the STM image shows the emergence of atomically isolated islands (S1 phase) formed on the Ag(111) surface. Increasing the boron coverage, the 2D boron island can extend in size until it covers the entire surface. High-resolution STM images in Figure 3b reveal the ordered parallel stripes of the S1 phase, which is attributed to a Moiré pattern resulting from the mismatching between the lattices of borophene and Ag(111)

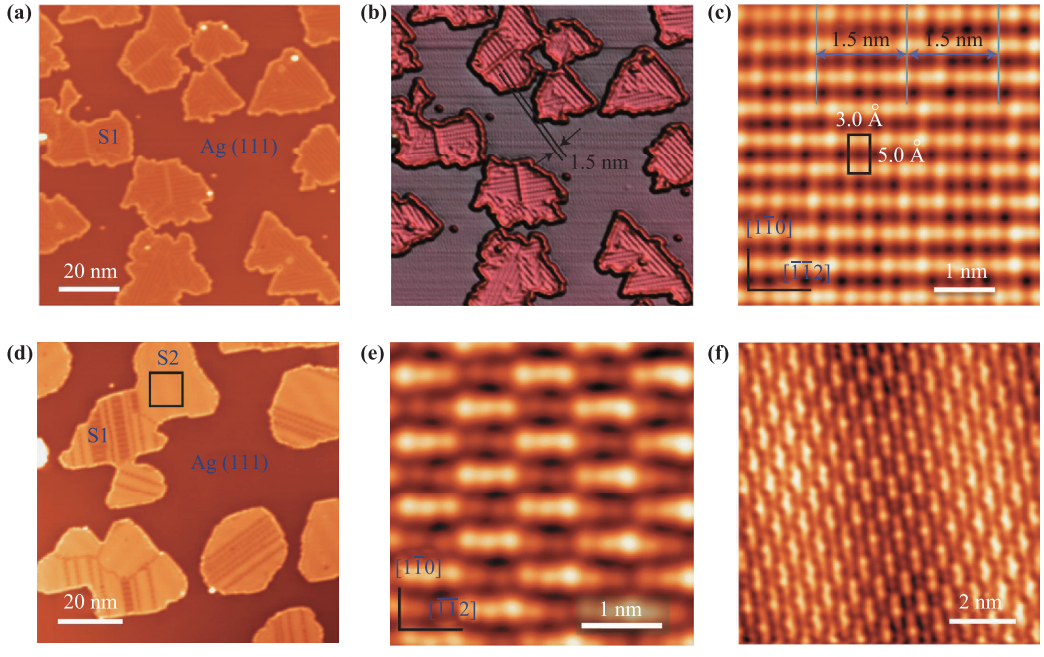

Fig. 3 Experimentally synthesized 2D boron sheets on Ag(111). **(a)** STM topographic image of boron structures on Ag(111), with a substrate temperature of $\sim$ 570 K during growth. The boron islands are labelled as the "S1" phase. **(b)** Three-dimensional version of a, in which the stripes with 1.5 nm intervals are clearly resolved. **(c)** High-resolution STM image of S1 phases. The S1 unit cell is marked by a black rectangle, and the 1.5 nm stripes are indicated by solid lines. **(d)** STM image of boron sheets after annealing the surface to 650 K. The two different phases are labelled "S1" and "S2". Most boron islands are transformed to the S2 phase, but the S1 phase still remains in small parts of the islands. **(e)** STM image obtained on the area marked by the black rectangle in (d). **(f)** High-resolution STM image of the S2 phase, zoomed in from (e). Note that the image is rotated to allow comparison with (c). Bias voltages of STM images: −4.0 V (a, b), 0.9 V (c), −4.0 V (d), and 1.0 V (e, f). Reproduced from Ref. [50].

The atomically resolved STM image shown in Fig. 3(c) indicates the unit cell of the S1 phase (marked by the black rectangle), in which the distance between nearest-neighbour bright protrusions is 3.0 Å along the rows and 5.0 Å perpendicular to the rows. Another phase of borophene (named S2) transforming from the S1 phase was observed by annealing the sample above 650 K or growing boron atoms directly with a substrate temperature of ∼ 680 K. The high-resolution STM images in Figs. 3(e) and (f) indicate that the S2 phase also consists of parallel rows of protrusions in the $[\bar{1}\bar{1}2]$ direction of the Ag(111) substrate. The distance between nearest-neighbor protrusions is 3.0 Å along the rows, and 4.3 Å across the rows. Another obvious feature is that the protrusions along the rows are divided into sections with alternative brighter and darker protrusions, and each section involves five protrusions. The growth of two different phases on Ag(111) further verifies the polymorphic nature of 2D boron.

Besides S1 and S2 phases, which covered most of the area of Ag(111), two additional structures of borophene of a smaller area were found and reported by Zhong *et al.* [52]. As shown in Figs. 4(a) and (b), the new S3 phase in the middle and top left of the image features a smooth surface with many bright domain boundaries, different from the ordered striped row on the S1 islands. But the high-resolution STM images given in Fig. 4(c) show that the S3 phase has the same rectangular lattice as that of the S1 phase. On the other hand, another new boron S4 phase with hexagonal symmetry on Ag(111) [shown in Figs. 4(d) and (f)] has a rhombic unit cell with a side length of 5.2 Å. The periodicity is very close to that of the long-expected α-sheet.

Around the same time, Mannix and coworkers also synthesized monolayer boron islands on Ag(111) surfaces by the MBE method [51]. The atomically thin boron reported by Mannix *et al.* also exhibits two different morphologies, which are identified as the striped and homogeneous phases [Fig. 5(b)]. STM characterization revealed that the final product depended on the deposition rate. At a low deposition rate corresponding to low boron coverage, a flat striped phase consisting of a rectangular lattice dominated the surface [Fig. 5(c)]. At higher deposition rates, more homogeneous islands were observed as periodically protruding atomic chains [Fig. 5(d)]. Despite some differences in the details (owing to the different bias voltages used for STM imaging), this sheet does resemble the S2 phase described by Feng *et al.* [50]. Meanwhile, the form of the striped phase was also temperature dependent. On increasing the substrate temperature, the initial flat striped phase can transform into a new striped phase with periodic

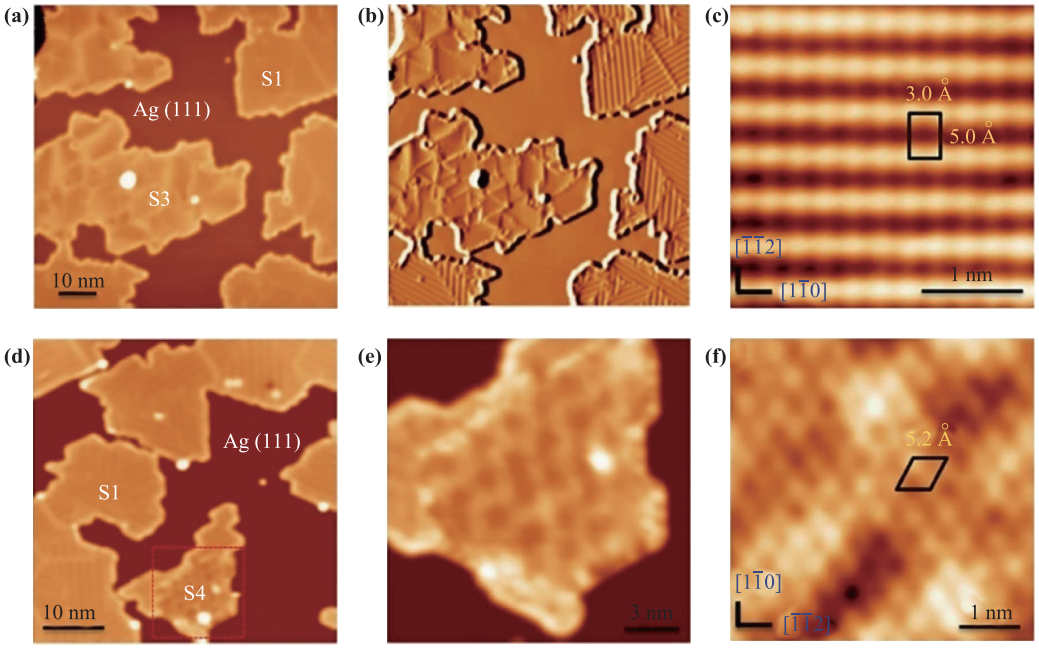

Fig. 4 STM images of two metastable 2D boron sheets on Ag(111). **(a)** STM topographic image of boron structures on Ag(111). The boron islands are labelled as "S1" and "S3" phases. **(b)** The derivative STM image of (a). **(c)** High-resolution STM image of the S3 phases. The S3 unit cell is marked by a black rectangle. **(d)** STM topographic image of boron structures on Ag(111). The boron islands are labelled as "S1" and "S4" phases. Most boron islands shown in the image are the S1 phase. **(e)** STM image obtained from the area marked by the red dotted rectangle in (d). **(f)** High-resolution STM image of the S4 phase. The S4 unit cell is marked by a black rhombus. Reproduced from Ref. [52].

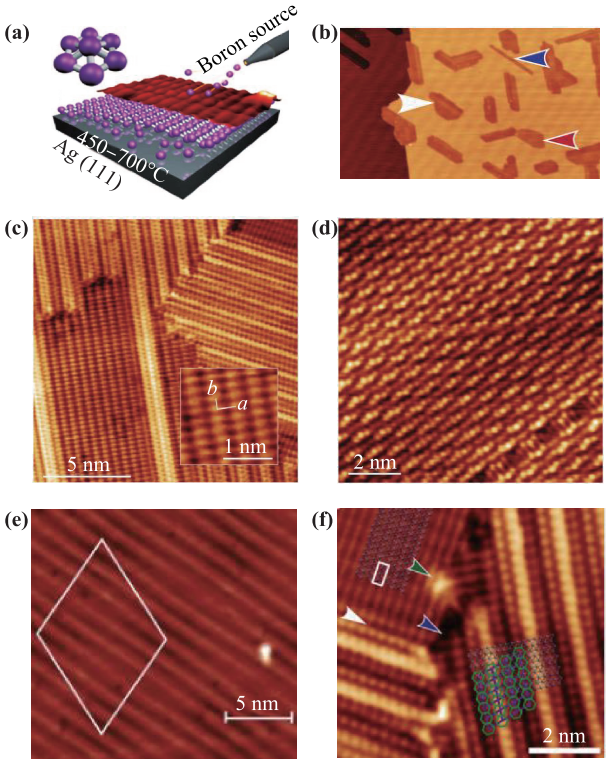

Fig. 5 Growth and atomic-scale characterization of borophene sheets. **(a)** Growth setup with boron source of MBE. **(b)** The STM image of mixed-phase borophene, where the white, red, and blue arrows denote striped, homogeneous, and striped nanoribbon phase regions, respectively. **(c)** Atomically resolved STM topography image of striped phase, in which prominent stripe features structurally commensurate with rectangular lattice regions (inset; where a and b represent the lattice vectors) are visible. **(d)** Atomically resolved STM topography image of homogeneous phase. **(e)** STM topography image of the undulated boron sheet on Ag(111) with Moiré pattern, where the rhombic supercell is highlighted in white. **(f)** Atomic resolution image detailing the limited structural coherence and common structural motifs between the flat and undulated striped phases. Reproduced from Refs. [51, 53].

nanoscale corrugations, forming a ~ 8 nm rhombohedral Moiré pattern [Fig. 5(e)] [51, 53]. However, there are always regions with the flat striped structure consisting of a rectangular lattice within undulated striped phase domains [Fig. 5(f)]. A detailed discussion of the undulated phase will be presented in the next section.

2.2 Borophene nanoribbons

Inspired by the experimental synthesis of borophene, the 1D boron nanostructures are also expected to be made with controllable and clean methods. Just like the graphene nanoribbons, the 1D borophene nanoribbons may also exhibit improved properties for building nanodevices. Indeed, in our previous study on the growth of 2D borophene, the STM images revealed borophene islands that show a predominantly triangular shape and edges along the crystallographic orientations of Ag(111), indicating the template effect of the substrate. It is intuitive that the shape of 2D boron sheets can be controlled by the anisotropy of the substrate. Zhong *et al.* [54] grew boron atoms on an anisotropic metal substrate — Ag(110) — and found single-atom-thick borophene nanoribbons (BNRs) successful synthesized on it. All the ribbons are along the $[\bar{1}10]$ direction of Ag(110) and can run across the steps on the surface. The width of the ribbons is distributed in a narrow range between 10.3 ± 0.2 nm. High-resolution STM images revealed four ordered surface structures in BNRs, named P1, P2, P3, and P4 respectively for the sake of simplicity (Fig. 6). As displayed in Fig. 6(a), the unit cell of P1 is rectangular with the long side along the $[\bar{1}10]$ direction of Ag(110). Besides, Figs. 6(b) and (c) show that the long sides of the unit cells of P2 and P3 are along the $[\bar{1}10]$ direction of Ag(110), indicating they are in mirror symmetry to each other. As for P4 phases, the STM image shows a unit cell with a rotational angle of 30° to the $[\bar{1}10]$ direction of substrate. Their results further confirmed the

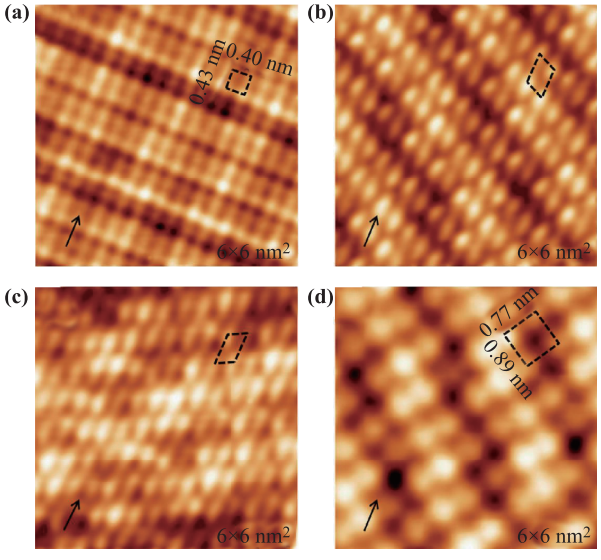

Fig. 6 High-resolution STM images of boron nanoribbons on Ag(110). **(a–d)** High-resolution STM images for P1–P4, respectively. The unit cells of P1–P4 are marked by different dotted patterns. The size of the unit cells can be listed as follows: $a = 0.40$ nm, $b = 0.43$ nm, $\phi = 90$ for P1; $a = 0.44$ nm, $b = 0.82$ nm, $\phi = 61°$ for P2; $a = 0.45$ nm, $b = 0.76$ nm, $\phi = 60°$ for P3; and $a = 0.89$ nm, $b = 0.77$ nm, $\phi = 90°$ for P4. The $[-110]$ direction of Ag(110) is marked by black arrows in the images. The images are 6×6 nm^2 in size. The bias voltages of STM images are -1.7 V for (a) and (b) and -1.6 V for (c) and (d). Reproduced from Ref. [54].

inherent polymorphism of 2D boron. These high-quality BRNs suggested that the presence of 2D boron sheets may be determined using many factors, such as substrate temperature, deposition and the crystallographic orientations of substrate.

3 Atomic structures of synthesized 2D boron

As mentioned above, Feng *et al.* observed the formation of two sheets, referred to as the S1 and S2 phases. In order to elucidate the fact that the synthesized monolayer boron films are the long-expected borophene, they performed independent theoretical work to determine the atomic structures of these new phases. First of all, they investigated a large number of 2D boron structures from previous theoretical predictions, and then compared the experimental periodicities of the two phases with theoretical values. As a result, β_{12} sheets share the same periodicity as S1, while the unit cell of the S2 phase is identical to that of the χ_3 sheet predicted by theoretical calculations. To confirm the atomic structures, first-principle calculations were performed on these two sheets on the Ag(111) surface. The β_{12} sheet was placed on Ag(111) with the boron rows in the [$\bar{1}$12] direction of the Ag(111) surface, as shown in Fig. 7(a). After relaxation, the geometric structure of β_{12} remains planar [Fig. 7(b)]. From the simulated STM image in Fig. 7(c), we can see that the β_{12} sheet is in excellent agreement with the S1 phase, in terms of topography, rectangular lattice and the Moiré pattern. On the other hand, the χ_3 sheet consisting of narrower zigzag boron rows separated by hole arrays is proposed for the S2 phase [Figs. 7(d) and (e)]. A simulated STM image [Fig. 7(f)] reveals alternating bright/dark protrusions along the rows, agreeing perfectly with our STM observations. It should be noted that the atomic structures of the β_{12} sheet and χ_3 sheet on Ag(111) remain planar; thus, the patterns in STM images are attributed to inhomogeneous electronic interactions with the substrate. Such charge inhomogeneity comes from the matching between the boron lattices and the Ag(111) lattice, which results in a different arrangement of the boron atoms on the Ag(111) lattice, especially along the boron row. By means of essentially the same method, the S3 and S4 phases should be the β_{12} and α sheet respectively. The calculated results of these structures on Ag(111) based on the first-principle theory are illustrated in Figs. 7(g) and (j). S3 is also the β_{12} sheet, the same as the S1 phase, but with a distinct rotational relationship with the Ag(111) substrate. The rotation of the β_{12} sheet with respect to Ag(111) leads to perfect lattice matching between the film and substrate; subsequently, no obvious Moiré patterns are observed in the S3 phase. What needs to be emphasized is that the S4 sheet, with a clear hexagonal symmetry, is the long-expected α sheet. Both proposed models of these new phases [Figs. 7(i) and (l)] give rise to simulated STM images in good agreement with experimental data [Figs. 4(e) and (f)].

It is a notable fact that the striped phase described in Ref. [51] closely resembles the S1 phase described by Feng *et al.* in Ref. [50] in terms of the rectangular lattice and STM images. However, a bulked triangular lattice with slight distortion along the buckled rows was ini-

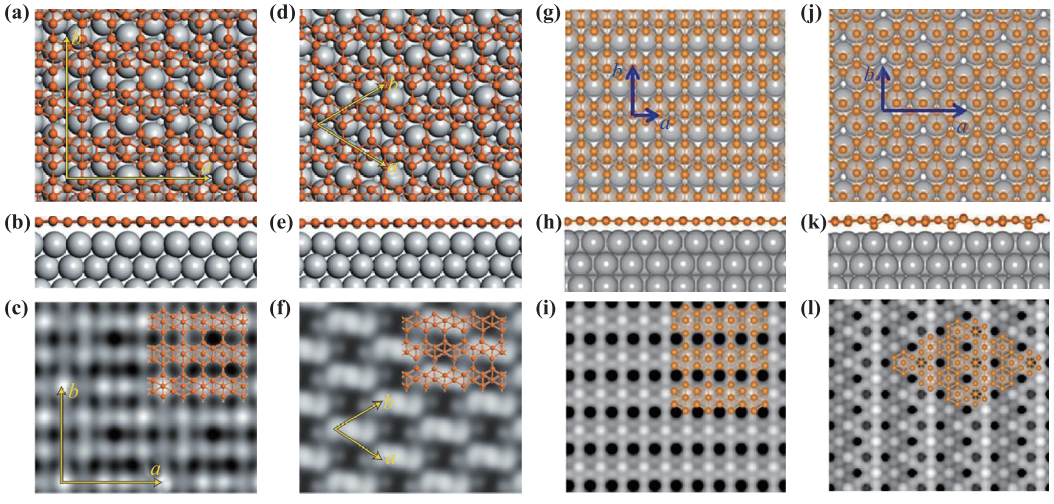

Fig. 7 Structure models of borophene on Ag(110) based on DFT calculations. **(a–c)** Atomic structure of the β_{12} sheet and simulated STM image, proposed for the S1 phase in Figs. 3(a–c). **(d–f)** Atomic structure of the χ_3 sheet and simulated STM image, proposed for the S2 phase in Figs. 3(d–f). **(g–i)** Atomic structure of the β_{12} sheet and simulated STM image, proposed for the S3 phase in Fig. 4(c). **(j–l)** Atomic structure of the α sheet and simulated STM image, proposed for the S4 phase in Fig. 4(f). Reproduced from Refs. [50, 52].

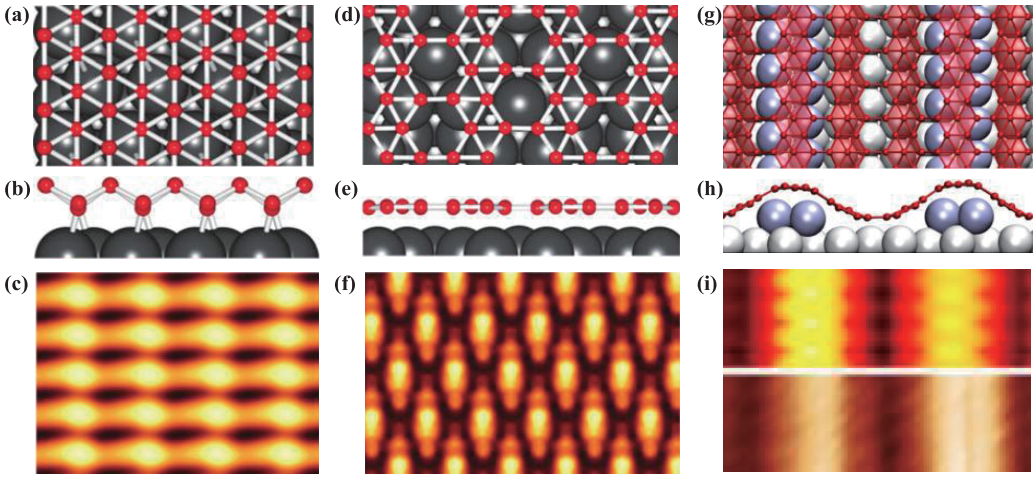

Fig. 8 Computational prediction of borophene structure and corresponding simulated STM images. **(a–c)** Atomic structure of a buckled triangular structure and simulated STM image, proposed for the striped phase in Fig. 5(c). **(d–f)** Atomic structure of the χ_3 sheet and simulated STM image, proposed for the homogeneous phase in Fig. 5(d). **(g–i)** Atomic structure of the β_{12} sheet on reconstructed Ag(111) and simulated STM image, proposed for the undulated striped phase in Figs. 5(e) and (f). Reproduced from Refs. [55, 57].

tially proposed as an atomic model for the striped phase [Figs. 8(a) and (b)]. The simulated STM image shown in Figure 8c also captures the key features of experimental images [the insert in Fig. 5(c)]. But a recent computational and experimental study [53] reported by Zhang *et al.* provides solid support for the β_{12} sheet. As mentioned in Section 2, the initial flat striped phase can transform into a new striped phase with periodic nanoscale corrugations at a higher substrate temperature. Zhang *et al.* [53] suggested that the corrugated striped phase is the β_{12} sheet on the reconstructed Ag(111) surface rather than the a closely packed triangular model [Figs. 8(g) and (h)]. The simulated STM [the top panel of Fig. 8(i)] image of this undulated β_{12} sheet shows excellent agreement with the STM characterization of the "wavy" configuration [bottom of Fig. 8(i)]. It may be that a structural transition from the triangular model to the β_{12} sheet occurs before the flat-to-corrugated transformation, but such a structural transition lacks evidence in view of the coherent atomic lattice across the interface between the corrugated and flat regions [Figs. 5(c) and (f)]. In addition, the earlier *ab initio* calculations by global minimum search also showed that the β_{12} sheet is the ground state on Ag(111) [55]. Besides, the β_{12} sheet matches the lattice constants of Ag(111) (only about 1% mismatch) better than the triangular sheet (about 3.1% off) and is also considerably more flexible with anisotropic high-bending flexibility than the triangular sheet with finite thickness. Although all this evidence tends to supports the β_{12} sheet as the atomic model for the S1 and striped phases, further experimental characterization and theoretical analyses are required to reach a firm conclusion.

The second phase proposed by Mannix *et al.*, referred to as the homogeneous phase, shows the same STM features as the S2 phase described by Feng *et al.* So, the homogeneous phase should have an atomic structure like the χ_3 sheet. Mannix *et al.* did not present the corresponding model in their initial report unit the recent review [56] after the description by Feng *et al.*

Similarly, first-principle calculations were also carried out to confirm the atomic structures of BNRs on these four phases on Ag(110), and the optimized atomic models are shown in Figs. 9(a)–(h). The P1, P2, P3 and P4 boron nanoribbons correspond to the χ_3, β, and β_8 sheet, respectively. From the side view of the optimized P1-P4 BNRs [Figs. 9(e)–(f)], only the χ_3 sheet remains completely planar, indicating high stability. The simulated STM of the χ_3 sheet shown in Fig. 9(i) reproduced both the striped feature and the unit cell in the STM image displayed in Fig. 6(a). The experimental STM images and the DFT calculations indicate that the P2 and P3 phases can both be explained by the β structure, but with mirror-symmetric orientations with respect to Ag(110), as shown in Figs. 9(b) and (c). In contrast to the perfectly planar configuration in P1, the β boron sheet is slightly buckled on Ag(110) due to the interfacial interactions, as displayed in Figs. 9(f) and (g). It is the buckled structure with different boron atom height that results in the protrusions with a different brightness in STM images [Figs. 6(b) and (c)]. Consequently, the simulated STM data displayed in Figs. 9(j) and (k) concur with experimental images. The β_8 sheet predicted by Wu *et al.* [45] is proposed as an atomic model for the P4 phase. In spite of the larger fluctuation of the re-

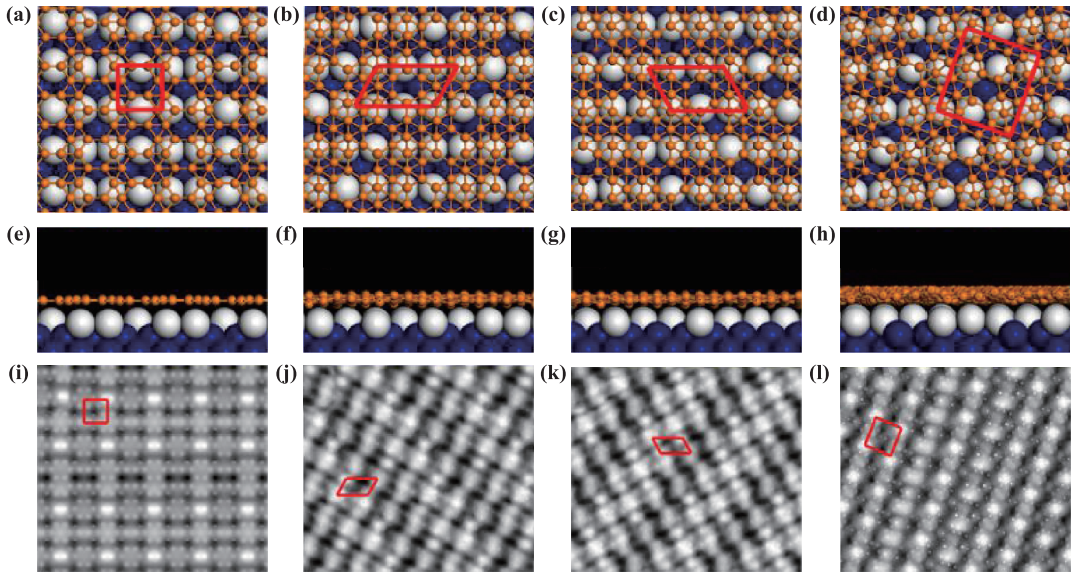

Fig. 9 Atomic structures of boron nanoribbons on Ag(110) optimized by DFT. **(a–d)** Top and **(e–h)** side views of optimized P1-P4 BNRs on Ag(110) surface, respectively. Color codes: B, small orange spheres; topmost Ag, large white spheres; and lower Ag, large blue spheres. **(i–l)** Simulated STM images for P1–P4 based on the calculated electronic density (0–2 eV above the Fermi level). The red frameworks correspond to the observed unit cells in STM images. Reproduced from Ref. [54].

laxed structure [Figs. 9(d) and (h)], the simulated STM image of the β_8 sheet [Fig. 9(i)] is also in good agreement with experimental ones [Fig. 6(d)]. All these four kinds of phases as nanoribbons have a similar probability of forming on the anisotropic Ag(110) surface during growth, owing to the similar formation energies. Surprisingly, these four kinds of structures share common features: they consist of full-filled boron chains separated by single rows of hexagonal holes. The full-filled boron chains act as "donors" while the hexagon holes act as "acceptors", which are mixed in such a way as to compensate the electron deficiency of boron and make the 2D boron sheet more stable.

4 Summary

Recent advances in the experimental synthesis and characterization of 2D boron have been introduced in this review. In addition, we particularly focus on the plausible structural model and the structural polymorphism of the successfully realized borophene in experiments. Being the fifth element, boron offers more puzzles in its structural organization than its neighbors in the periodic table, because it is has an electron-deficient atom and the number of valence electrons is lower than that of available orbitals. This causes boron to form the planar 2D borophene and BNRs through the coexistence of localized 2c-2e and delocalized multicenter two-electron (nc-2e) bonds. In particular, the successful fabrication of the monolayer borophene on metal substrates paves the way to exploring boron-based microelectronic device applications. It is worth mentioning that the electronic properties of borophene are also important and intriguing, albeit beyond the scope of this brief review. Further details on the electronic properties of the successfully synthesized β_{12} and χ_3 structures can be found in Refs. [58–60]. It should also be stressed that the unambiguous metallicity of 2D boron may complement the shortage of existing 2D materials and open possibility to making boron a core material for future nanodevices.

Acknowledgements This work was supported by the Ministry of Science and Technology of China (Grant Nos. 2016YFA0300904, 2016YFA0202301, 2013CBA01601, and 2013CB921702), the National Natural Science Foundation of China (Grant Nos. 11761141013, 11674366, and 11674368), and the Strategic Priority Research Program of the Chinese Academy of Sciences (Grant Nos. XDB07020100 and XDPB06).

References and notes

1. K. S. Novoselov, A. K. Geim, S. V. Morozov, D. Jiang, Y. Zhang, S. V. Dubonos, I. V. Grigorieva, and A. A. Firsov, Electric field effect in atomically thin carbon films, *Science* 306(5696), 666 (2004)
2. D. Akinwande, L. Tao, Q. Yu, X. Lou, P. Peng, and D. Kuzum, Large-area graphene electrodes: Using CVD to facilitate applications in commercial touchscreens, flex-

ible nanoelectronics, and neural interfaces, *IEEE Nanotechnol. Mag.* 9(3), 6 (2015)

3. A. C. Ferrari, F. Bonaccorso, V. Fal'ko, K. S. Novoselov, S. Roche, et al., Science and technology roadmap for graphene, related two-dimensional crystals, and hybrid systems, *Nanoscale* 7(11), 4598 (2015)
4. G. Fiori, F. Bonaccorso, G. Iannaccone, T. Palacios, D. Neumaier, A. Seabaugh, S. K. Banerjee, and L. Colombo, Electronics based on two-dimensional materials, *Nat. Nanotechnol.* 9(10), 768 (2014)
5. A. L. Ivanovskii, Graphene-based and graphene-like materials, *Russ. Chem. Rev.* 81(7), 571 (2012)
6. S. Balendhran, S. Walia, H. Nili, S. Sriram, and M. Bhaskaran, Elemental analogues of graphene: Silicene, germanene, stanene, and phosphorene, *Small* 11(6), 640 (2015)
7. J. Zhao, H. Liu, Z. Yu, R. Quhe, S. Zhou, Y. Wang, C. C. Liu, H. Zhong, N. Han, J. Lu, Y. Yao, and K. Wu, Rise of silicene: A competitive 2D material, *Prog. Mater. Sci.* 83, 24 (2016)
8. B. Feng, Z. Ding, S. Meng, Y. Yao, X. He, P. Cheng, L. Chen, and K. Wu, Evidence of silicene in honeycomb structures of silicon on Ag(111), *Nano Lett.* 12(7), 3507 (2012)
9. P. Vogt, P. De Padova, C. Quaresima, J. Avila, E. Frantzeskakis, M. C. Asensio, A. Resta, B. Ealet, and G. Le Lay, Silicene: compelling experimental evidence for graphene-like two-dimensional silicon, *Phys. Rev. Lett.* 108(15), 155501 (2012)
10. A. Fleurence, R. Friedlein, T. Ozaki, H. Kawai, Y. Wang, and Y. Yamada-Takamura, Experimental evidence for epitaxial silicene on diboride thin films, *Phys. Rev. Lett.* 108(24), 245501 (2012)
11. J. Gou, Q. Zhong, S. Sheng, W. Li, P. Cheng, H. Li, L. Chen, and, K. Wu, Strained monolayer germanene with 1×1 lattice on Sb(111), *2D Materials* 3, 045005 (2016)
12. L. Li, S. Lu, J. Pan, Z. Qin, Y. Wang, Y. Wang, G. y. Cao, S. Du, and H. J. Gao, Buckled germanene formation on Pt(111), *Adv. Mater.* 26(28), 4820 (2014)
13. S. Cahangirov, M. Topsakal, E. Aktürk, H. Şahin, and S. Ciraci, Two- and one-dimensional honeycomb structures of silicon and germanium, *Phys. Rev. Lett.* 102(23), 236804 (2009)
14. J. Gou, L. Kong, H. Li, Q. Zhong, W. Li, P. Cheng, L. Chen, and K. Wu, Strain-induced band engineering in monolayer stanene on Sb(111), *Phys. Rev. Mater.* 1(5), 054004 (2017)
15. F.-F. Zhu, W.-J. Chen, Y. Xu, C.-L. Gao, D.-D. Guan, C.-H. Liu, D. Qian, S.-C. Zhang, and J.-F. Jia, Epitaxial growth of two-dimensional stanene, *Nature Mater.* 14, 1020 (2015)
16. Y. Xu, B. Yan, H. J. Zhang, J. Wang, G. Xu, P. Tang, W. Duan, and S. C. Zhang, Large-gap quantum spin Hall insulators in thin films, *Phys. Rev. Lett.* 111(13), 136804 (2013)
17. C. C. Liu, H. Jiang, and Y. Yao, Low-energy effective Hamiltonian involving spin-orbit coupling in silicene and two-dimensional germanium and tin, *Phys. Rev. B* 84(19), 195430 (2011)
18. A. Molle, J. Goldberger, M. Houssa, Y. Xu, S. C. Zhang, and D. Akinwande, Buckled two-dimensional Xene sheets, *Nat. Mater.* 16(2), 163 (2017)
19. K. Takeda and K. Shiraishi, Theoretical possibility of stage corrugation in Si and Ge analogs of graphite, *Phys. Rev. B* 50(20), 14916 (1994)
20. K. H. Wu, A review of the growth and structures of silicene on Ag(111), *Chin. Phys. B* 24(8), 086802 (2015)
21. H. J. Zhai, B. Kiran, J. Li, and L. S. Wang, Hydrocarbon analogues of boron clusters — planarity, aromaticity and antiaromaticity, *Nat. Mater.* 2(12), 827 (2003)
22. A. P. Sergeeva, I. A. Popov, Z. A. Piazza, W. L. Li, C. Romanescu, L. S. Wang, and A. I. Boldyrev, Understanding boron through size-selected clusters: Structure, chemical bonding, and fluxionality, *Acc. Chem. Res.* 47(4), 1349 (2014)
23. W. L. Li, Q. Chen, W. J. Tian, H. Bai, Y. F. Zhao, H. S. Hu, J. Li, H. J. Zhai, S. D. Li, and L. S. Wang, The B35 cluster with a double-hexagonal vacancy: A new and more flexible structural motif for borophene, *J. Am. Chem. Soc.* 136(35), 12257 (2014)
24. Z. A. Piazza, H. S. Hu, W. L. Li, Y. F. Zhao, J. Li, and L. S. Wang, Planar hexagonal B_{36} as a potential basis for extended single-atom layer boron sheets, *Nat. Commun.* 5, 3113 (2014)
25. W. Huang, A. P. Sergeeva, H. J. Zhai, B. B. Averkiev, L. S. Wang, and A. I. Boldyrev, A concentric planar doubly-aromatic B_{19} cluster, *Nat. Chem.* 2(3), 202 (2010)
26. H. J. Zhai, Y. F. Zhao, W. L. Li, Q. Chen, H. Bai, H. S. Hu, Z. A. Piazza, W. J. Tian, H. G. Lu, Y. B. Wu, Y. W. Mu, G. F. Wei, Z. P. Liu, J. Li, S. D. Li, and L. S. Wang, Observation of an all-boron fullerene, *Nat. Chem.* 6(8), 727 (2014)
27. J. Lv, Y. Wang, L. Zhu, and Y. Ma, B_{38}: An all-boron fullerene analogue, *Nanoscale* 6(20), 11692 (2014)
28. H. Li, N. Shao, B. Shang, L. F. Yuan, J. Yang, and X. C. Zeng, Icosahedral B_{12}-containing core–shell structures of B_{80}, *Chem. Commun.* 46(22), 3878 (2010)
29. N. G. Szwacki, A. Sadrzadeh, and B. I. Yakobson, B_{80} fullerene: An *ab initio* prediction of geometry, stability, and electronic structure, *Phys. Rev. Lett.* 98(16), 166804 (2007)
30. J. Zhao, L. Wang, F. Li, and Z. Chen, B_{80} and other medium-sized boron clusters: Core-shell structures, not hollow cages, *J. Phys. Chem. A* 114(37), 9969 (2010)
31. D. Ciuparu, R. F. Klie, Y. Zhu, and L. Pfefferle, Synthesis of pure boron single-wall nanotubes, *J. Phys. Chem. B* 108(13), 3967 (2004)

32. J. Tian, Z. Xu, C. Shen, F. Liu, N. Xu, and H. J. Gao, One-dimensional boron nanostructures: Prediction, synthesis, characterizations, and applications, *Nanoscale* 2(8), 1375 (2010)

33. A. K. Singh, A. Sadrzadeh, and B. I. Yakobson, Probing properties of boron α-tubes by *ab initio* calculations, *Nano Lett.* 8(5), 1314 (2008)

34. T. Ogitsu, E. Schwegler, and G. Galli, β-rhombohedral boron: At the crossroads of the chemistry of boron and the physics of frustration, *Chem. Rev.* 113(5), 3425 (2013)

35. J. K. Olson and A. I. Boldyrev, Electronic transmutation: Boron acquiring an extra electron becomes 'carbon', *Chem. Phys. Lett.* 523, 83 (2012)

36. S. Saxena, Introduction to Boron Nanostructures, *Handbook of Boron Nanostructures*, 1 (2016)

37. I. Boustani, Systematic ab initio investigation of bare boron clusters: mDetermination of the geometryand electronic structures of B_n (n = 2–14), *Phys. Rev. B* 55(24), 16426 (1997)

38. I. Boustani, New quasi-planar surfaces of bare boron, *Surf. Sci.* 370(2–3), 355 (1997)

39. K. C. Lau and R. Pandey, Stability and electronic properties of atomistically-engineered 2D boron sheets, *J. Phys. Chem. C* 111(7), 2906 (2007)

40. K. C. Lau, R. Pati, R. Pandey, and A. C. Pineda, First-principles study of the stability and electronic properties of sheets and nanotubes of elemental boron, *Chem. Phys. Lett.* 418(4–6), 549 (2006)

41. I. Cabria, M. López, and J. Alonso, Density functional calculations of hydrogen adsorption on boron nanotubes and boron sheets, *Nanotechnology* 17(3), 778 (2006)

42. H. Tang and S. Ismail-Beigi, Self-doping in boron sheets from first principles: A route to structural design of metal boride nanostructures, *Phys. Rev. B* 80(13), 134113 (2009)

43. H. Tang and S. Ismail-Beigi, Novel precursors for boron nanotubes: The competition of two-center and three-center bonding in boron sheets, *Phys. Rev. Lett.* 99(11), 115501 (2007)

44. H. Tang and S. Ismail-Beigi, First-principles study of boron sheets and nanotubes, *Phys. Rev. B* 82(11), 115412 (2010)

45. X. Wu, J. Dai, Y. Zhao, Z. Zhuo, J. Yang, and X. C. Zeng, Two-dimensional boron monolayer sheets, *ACS Nano* 6(8), 7443 (2012)

46. E. S. Penev, S. Bhowmick, A. Sadrzadeh, and B. I. Yakobson, Polymorphism of two-dimensional boron, *Nano Lett.* 12(5), 2441 (2012)

47. Y. Liu, E. S. Penev, and B. I. Yakobson, Probing the synthesis of two-dimensional boron by first-principles computations, *Angew. Chem. Int. Ed.* 52(11), 3156 (2013)

48. H. Liu, J. Gao, and J. Zhao, From boron cluster to two-dimensional boron sheet on Cu(111) surface: Growth mechanism and hole formation, *Sci. Rep.* 3(1), 3238 (2013)

49. L. Zhang, Q. Yan, S. Du, G. Su, and H. J. Gao, Boron sheet adsorbed on metal surfaces: Structures and electronic properties, *J. Phys. Chem. C* 116(34), 18202 (2012)

50. B. Feng, J. Zhang, Q. Zhong, W. Li, S. Li, H. Li, P. Cheng, S. Meng, L. Chen, and K. Wu, Experimental realization of two-dimensional boron sheets, *Nat. Chem.* 8(6), 563 (2016)

51. A. J. Mannix, X. F. Zhou, B. Kiraly, J. D. Wood, D. Alducin, B. D. Myers, X. Liu, B. L. Fisher, U. Santiago, J. R. Guest, M. J. Yacaman, A. Ponce, A. R. Oganov, M. C. Hersam, and N. P. Guisinger, Synthesis of borophenes: Anisotropic, two-dimensional boron polymorphs, *Science* 350(6267), 1513 (2015)

52. Q. Zhong, J. Zhang, P. Cheng, B. Feng, W. Li, S. Sheng, H. Li, S. Meng, L. Chen, and K. Wu, Metastable phases of 2D boron sheets on Ag(111), *J. Phys. Condens. Matter* 29(9), 095002 (2017)

53. Z. Zhang, A. J. Mannix, Z. Hu, B. Kiraly, N. P. Guisinger, M. C. Hersam, and B. I. Yakobson, Substrate-induced nanoscale undulations of borophene on silver, *Nano Lett.* 16(10), 6622 (2016)

54. Q. Zhong, L. Kong, J. Gou, W. Li, S. Sheng, S. Yang, P. Cheng, H. Li, K. Wu, and L. Chen, Synthesis of borophene nanoribbons on Ag(110) surface, arXiv: 1704.05603 (2017)

55. Z. Zhang, Y. Yang, G. Gao, and B. I. Yakobson, Two-Dimensional Boron Monolayers Mediated by Metal Substrates, *Angew. Chem. Int. Ed.* 54(44), 13022 (2015)

56. A. J. Mannix, B. Kiraly, M. C. Hersam, and N. P. Guisinger, Synthesis and chemistry of elemental 2D materials, *Nature Rev. Chem.* 1, 0014 (2017)

57. Z. Zhang, E. S. Penev, and B. I. Yakobson, Two-dimensional boron: Structures, properties and applications, *Chem. Soc. Rev.* 46(22), 6746 (2017)

58. B. Feng, O. Sugino, R. Y. Liu, J. Zhang, R. Yukawa, M. Kawamura, T. Iimori, H. Kim, Y. Hasegawa, H. Li, L. Chen, K. Wu, H. Kumigashira, F. Komori, T.C. Chiang, S. Meng, and I. Matsuda, Dirac fermions in borophene, *Phys. Rev. Lett.* 118(9), 096401 (2017)

59. B. Feng, J. Zhang, S. Ito, M. Arita, C. Cheng, L. Chen, K. Wu, F. Komori, O. Sugino, and K. Miyamoto, Discovery of 2D anisotropic Dirac cones, *Adv. Mater.* 30(2),1704025 (2018)

60. B. Feng, J. Zhang, R. Y. Liu, T. Iimori, C. Lian, H. Li, L. Chen, K. Wu, S. Meng, F. Komori, and I. Matsuda, Direct evidence of metallic bands in a monolayer boron sheet, *Phys. Rev. B* 94(4), 041408 (2016)